

Entanglement signatures of phase transition in higher-derivative quantum field theories II: Applications to lower dimensional systems

S. Santhosh Kumar* and S. Shankaranarayanan†
*School of Physics, Indian Institute of Science Education and
 Research Thiruvananthapuram (IISER-TVM), Kerala -695 016, India*

We explicitly show that sixth order spatial derivative, Lorentz symmetry violating term in two dimensional space leads to quantum phase transition. We show that around the critical point, the number of zero modes increase dramatically that catalyze the change in the ground state property of the many-body wave function. We extend the analysis to three dimensional cylindrical geometry and show that the entanglement heat-capacity has similar profile to the heat capacity measurements of high temperature superconductors. We explicitly show that the long-range interaction in the two dimensional surface explain key features of high temperature superconductors.

PACS numbers: 11.10.z, 03.65.Ud, 04.70.Dy, 05.30.Rt

I. INTRODUCTION

Landau theory of phase transition is a symmetry-based analysis of equilibrium behavior near a phase transition [1]. It is highly successful in many fields of condensed matter physics, including structural phase transitions, magnetism and superconductivity within Landau-Ginzburg-Wilson (LGW) paradigm [2]. There has been a lot of interest to understand the validity of the Landau-Ginzburg-Wilsonian paradigm for quantum phase transitions (QPT) — transitions at absolute zero temperature. Unfortunately, for certain cases, quantum mechanical generalization of LGW functional failed to explain quantum critical phenomena [3, 4].

As yet, no mathematical framework has been developed to have a fundamental understanding of the following features of QPT: (i) QPT are governed by coherent quantum fluctuations resulted from Heisenberg's uncertainty principle, leading to an abrupt change in the ground state properties of a many body system [5–13] and the transition from one quantum phase to another is brought about due to the changes in the external parameter of the system. (ii) As like classical phase transition, at quantum critical point (QCP), there are long-range correlations in the system [8, 11, 12] and strongly entangled [10, 14]. Hence, it is expected that quantum entanglement across regions may play crucial role at QCP [6, 9, 15, 16].

To overcome the complexity of the interactions underlying QPTs, theoretical work has focused on one-dimensional quantum systems [10–12, 17]. In this work, we study the effect of higher derivative field theories and provide concrete example of a QPT which lies outside the LGW paradigm. The interesting features of the model are as follows: (i) It corresponds to free field theory and hence one can compute all the relevant quantities analyt-

ically. (ii) Usually, phase transitions are associated with non-linear terms however, the current model shows QPT due to linear, higher derivative terms. (iii) At QCP, long range interactions change the ground state properties of the many body system. (iv) The celebrated entanglement entropy-area law is valid for systems having local interactions [18–20]. We show yet another violation of area law for the case of next-to-next-nearest neighbor interactions leading to QPT.

Although there is yet no fundamental understanding on the role of quantum correlations, there is a huge body of work to identify quantifying tools indicating quantum criticality [21, 22]: (i) At QCP, quantum fidelity drastically changes due to the external parameter (P) thus signifying the notion of quantum order parameter [23]. (ii) Given a pure bipartite many particle ground state $\psi_{\text{GS}}(P) \in \mathcal{H}$ (Hilbert space), the associated reduced density operator matrix of its subsystem can be written always as $\rho = \exp(-H_E)$ [24], where H_E is the entanglement Hamiltonian of any one of the subsystem. It has been shown that entanglement spectrum contains more information than the entanglement entropy [25, 26]. In particular, at QCP, there is a finite ‘energy gap’ of H_{Ent} [27–29].

We extend the analysis to 3-dimensional cylindrical geometry and show that sixth-derivative leads to QPT. Interestingly, we show that the entanglement heat capacity shows a similar profile as the specific heat capacity of high temperature superconductors [30]. High temperature superconductors (HTS) are characterized by a layered, two-dimensional superconducting condensate and have features [31] that are very different from conventional superconducting metals. The two-dimensionality is evidenced by large anisotropies in the normal and superconducting electronic transport, and non-metallic transport in the direction perpendicular to the layered crystal structure. To take into account all these features of HTS, we have assumed that the long range interaction is in the 2-D plane while the interaction is short ranged in the perpendicular direction. We discuss the implications of our work for HTS.

*email: santhu@iisertvm.ac.in

†email: shanki@iisertvm.ac.in

II. MODEL SETUP AND METHOD

We consider the following 2-dimensional Hamiltonian

$$H = \frac{1}{2} \int d^2 \mathbf{r} \left[\Pi^2 - \Phi \left(\nabla^2 - \frac{\epsilon}{\kappa^2} \nabla^4 + \frac{\tau}{\kappa^4} \nabla^6 \right) \Phi \right], \quad (1)$$

where Π is the canonical conjugate momenta of the scalar field Φ , ∇^2 is the Laplace operator in two dimensional circular coordinates \mathbf{r} , ∇^4 and ∇^6 are the higher order spatial operators of the circular coordinates, ϵ and τ are dimensionless constants (and take values 0 or 1), κ is a constant which sets the scale for the deviation from Lorentz invariance and the speed of propagation is set to unity. Below, we briefly discuss some of the salient features of the model: (i) The above Hamiltonian corresponds to free field with a non-linear dispersion relation connecting frequency ω and wave number k via, $\omega^2 = k^2 + k^4/\kappa^2 + k^6/\kappa^4$. (ii) It is well-known that ∇^4 term with non-linear terms lead to Lifshitz transitions [32]. Here, we show that that ∇^6 terms drives QPT [33]. (iii) It is known that quantum fluctuations play an important role in lower dimensions, and almost invariably, destroy long-range order. Mermin-Wagner Theorem [34–36] precludes true long-range order in the thermodynamic limit at non-zero temperature in 1- and 2-dimensions. We show that, in 2-dimensions, next-to-next-nearest neighbor interactions introduces instability and drive quantum fluctuations leading to QPT.

As mentioned earlier, reduced density matrix (ρ) provides information about the strength of the quantum correlations across different regions. ρ is evaluated by tracing out the quantum degrees of freedom associated with the scalar order parameter inside a 2-D region of radius R . ρ can be computed semi-analytically by discretizing the Hamiltonian (1):

$$H(P) = \frac{1}{2a} \sum_{i,j=1, N, \infty}^{N, \infty} \left[\pi_{m,j}^2 \delta_{ji} + \varphi_{m,i} K_{ij}(P, m) \varphi_{m,j} \right] \quad (2)$$

where a is the discretization length scale, m is the azimuthal momentum quantum number, $\pi_{m,i}$ and $\varphi_{m,i}$ are dimensionless canonically commuting field operators obtain in a standard way from Π and Φ respectively, $P = 1/(\kappa a)^2$ is the dimensionless coupling parameter which determines the extend of deviation from the linear dispersion relation and K_{ij} is the interaction matrix [37]. Eq. (2) corresponds to N-coupled harmonic oscillators.

The procedure to obtain the entanglement entropy is similar to the one discussed in Ref. [33]. We assume that the quantum state corresponding to the Hamiltonian of the N-harmonic oscillator system is the ground state with wave-function $\psi_{\text{GS}}(x_1, \dots, x_n, t_1 \dots t_{N-n})$. $\rho(t, t')$ is obtained by tracing over the first n of the N oscillators. von Neumann entropy quantifies the ground state entanglement of a bipartite system via $S = -\text{Tr}(\rho \ln \rho)$ [38, 39].

III. RESULTS

A. Importance of sixth order derivative term

We compute the entanglement entropy numerically for the discretized Hamiltonian (2). The computations are done using Matlab for the lattice size $N = 600$, $10 \leq n \leq 590$ and the error in computation is 10^{-8} :

- (I) $\tau = 0, \epsilon = 1$ corresponding to the dispersion relation $\omega^2 = k^2 + k^4/\kappa^2$
- (II) $\tau = 1, \epsilon = 0$ corresponding to the dispersion relation $\omega^2 = k^2 + k^6/\kappa^4$
- (III) $\tau = 1, \epsilon = \pm 1$ corresponding to the dispersion relation $\omega^2 = k^2 \pm k^4/\kappa^2 + k^6/\kappa^4$

In the case of (I), like for canonical scalar field, the entanglement entropy is linearly related to n for all values of P hence, will not be presented in the main text [37]. The results for case (III) are similar to case (II), hence, we only present the results of case (II).

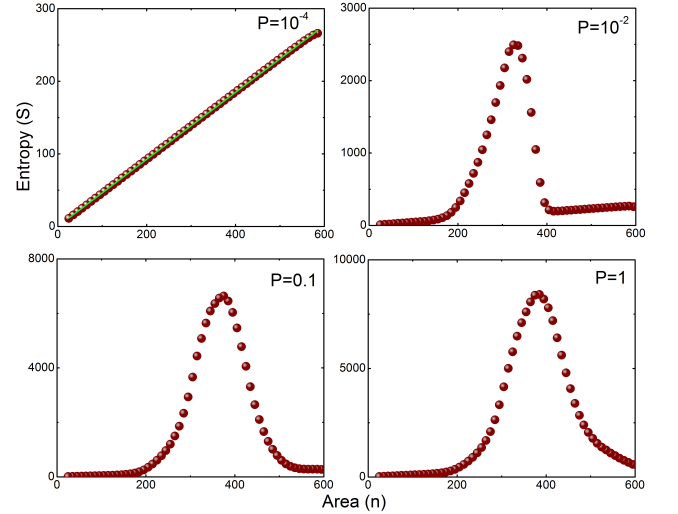


Fig. 1: Plots of entropy (S) versus area (n) for the scalar field with dispersion relation $\omega^2 = k^2 + k^6/\kappa^4$. Here we have plotted for different values of P . The brown dots are the numerical output data points and the green line is the best linear fit.

In Fig. (1) we have plotted S versus n for different values of the coupling constant P . The following points are interesting to note: First, the entropy profile changes as the coupling strength P is increased. In the case of $P = 10^{-4}$, the entropy is linearly related to n , however, as P increases the entropy-area linear relation is broken and the entropy changes by an order. It is interesting to see in the case of higher values of P , for large values of n the entropy scales linearly with area up to certain value of n and it is highly non-linear and for small values of n the entropy scales linearly with area. Second, it is known that the area-law is valid for gapped systems [20, 40].

It is important to note that even after the addition of higher derivative terms the system is gapped, however, the area-law is violated. Third, the area-law violation is generic feature for the Hamiltonian (2) containing sixth-derivative term. In other words, the area-law violation exists for all N 's [37].

The above results conclusively show that sixth derivative term lead to different quantum phases. To firmly identify what causes the change in the entropy by an order, in the rest of this work, we use three quantifying measures — Ground state fidelity, entanglement spectrum and many-body ground state energy — and show that this is indeed a QPT.

B. Ground state Fidelity and Energy

Ground state fidelity is defined as $F = \langle \psi_{\text{GS}}(P + \delta P) | \psi_{\text{GS}}(P) \rangle$, where δP is the infinitesimal change in the value of P [41, 42]. Sudden change in the overlap function indicates quantum criticality and hence it is a good quantitative measure to identify QCP [43–45].

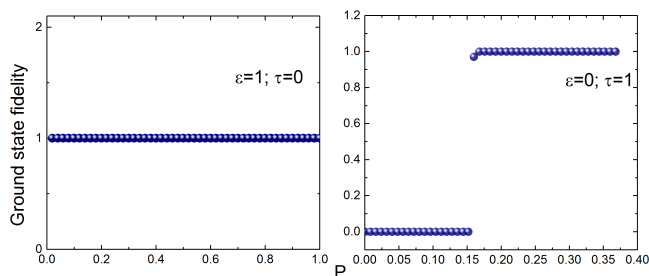


Fig. 2: Left plot is the ground state fidelity for case I ($\epsilon = 1, \tau = 0$) while the right plot is the ground state fidelity for case II ($\epsilon = 0, \tau = 1$). All plots are for $m = 0$ and $\delta P = 10^{-8}$.

In Fig. (2), overlap function is plotted for different coupling parameter P for the fourth and sixth derivative terms, from which we infer the following: (i) With the fourth derivative term the overlap function is always close to unity implying that the ground state many body wave functions for P and $P + \delta P$ are identical. This is consistent with the results of entanglement entropy that the entropy linearly scales with n for all values of P . (ii) With the sixth derivative term, the overlap function shows a sudden discontinuity close to $P = 0.17$. For $P > 0.17$, the ground state wave functions (as in the case of fourth derivative) for P and $P + \delta P$ are identical, however, for $P < 0.17$ ground state wave functions for P and $P + \delta P$ are orthogonal. This is also consistent with the results of entanglement entropy that entropy is non-linearly related to n . (iii) While the overlap function signals that the ground state wave function are not identical for P close of 0.17, entanglement entropy shows non-linear behavior even at $P = 0.01$. This also signals that the sixth order derivative term leads to instability and leads to different phases. It has been suggested that the signature

of QPT is also encoded in the many-body ground state of the system [18–20]. At the quantum criticality, ground state energy of the Hamiltonian $H(P)$ has a gap which is related to the correlation length of the system. In other words, gap becomes singular — developing infinite correlation length across the critical point [18–20].

In Fig. (3), the ground state energy of Hamiltonian $H(P)$ is plotted for different values of m for the fourth and sixth derivative terms (at constant P), from which we infer the following: (i) In the case of the fourth derivative term, the ground state vanishes only for $m = 0$. One can infer that only one zero mode is present. (ii) In the case of sixth derivative term, above the critical values of $P = 0.17$, several values of m have zero energy. One infers that multiple zero modes exist for all coupling constants above the critical $P = (P_c = 0.17)$. It is important to note that this critical point is different from the point in which the entropy-area law is violated ($P \simeq 10^{-2}$). In other words, entanglement entropy-area violation signals about a drastic change in the ground state behavior. Our model is yet another example of violation of area law in higher dimensions purely by the sixth order derivative term in the Hamiltonian.

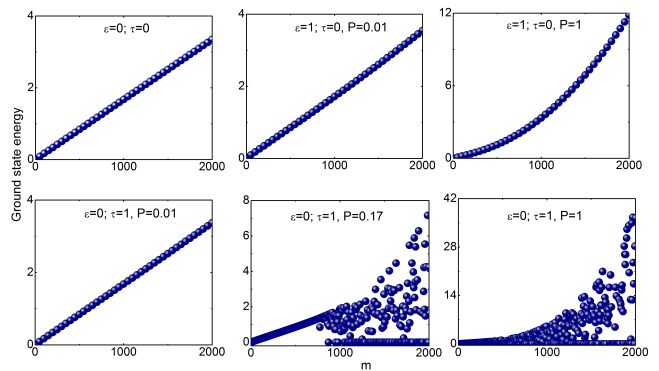


Fig. 3: Plots of ground state energy of $H(P)$ as a function of m . The first figure in the top panel for the canonical derivative term and the remaining two figures for case I ($\epsilon = 1, \tau = 0$) while the bottom panel is for case II ($\epsilon = 0, \tau = 1$).

C. Spectra of entanglement Hamiltonian

Reduced density matrix contains complete information on quantum entanglement, however, entanglement entropy being scalar may not provide complete information [25]. The entanglement Hamiltonian is an imaginary system that describes the correlations of the ground state. While it cannot be measured directly, it is related to the statistics of the fluctuations in the lattice. Entanglement Hamiltonian (H_E) is defined as $H_E = -\ln \rho$ and plays the role of βH in thermodynamic systems [25]. It has been shown that the largest and the second largest eigenvalues of H_E forms a gap at the QCP [25].

In Fig. (4), largest and the second largest eigenvalue of H_E are plotted for different coupling parameter P for the

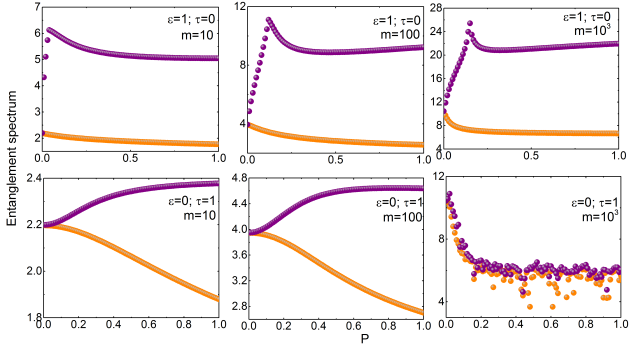


Fig. 4: Plots show the variation of the largest (orange) and second largest (purple) eigenvalues of the entanglement spectrum as a function P for different m values. The top panel is for case I ($\epsilon = 1, \tau = 0, n = 300$) while the bottom panel is for case II ($\epsilon = 0, \tau = 1, n = 300$).

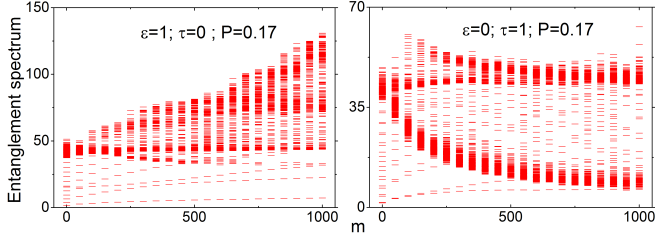


Fig. 5: Plots show the entanglement spectrum for the fourth order (left plot) and sixth order derivative (right plot) for $n = 300$.

fourth and sixth derivative terms, from which we infer the following: (i) In the case of fourth derivative term, the largest and the second largest eigenvalues of H_E have a gap for all values of the coupling constant except at $P = 0$. (ii) In the case of sixth derivative term, the largest and the second largest eigenvalues of H_E is degenerate for $P < 0.17$, however, above the critical point $P = 0.17$ the two eigenvalues are non-degenerate. (iii) The presence of the gap at a finite P provides an evidence of quantum critical point at $P = 0.17$. It is also interesting to note that it is at the same point that the overlap function also shows a sharp change [28].

Fig. (5) contains all the eigenvalues of the entanglement Hamiltonian H_E for the fourth order and sixth order derivative. The fingerprint of topological QPTs can be confirmed by the non collapsing of entanglement gap- the entanglement energy gap between the lowest and the highest entanglement part in the subsystem [25, 29, 46, 47]. It is interesting to note that the spectrum is continuous for the fourth order derivative term while it is discrete for the sixth order derivative term. In other words, sixth order derivative term brings a gap — that is absent in fourth order case — suggesting that the QPT is triggered by the linear scalar field and is topological in nature. This confirms the validity of Mermin-Wanger theorem.

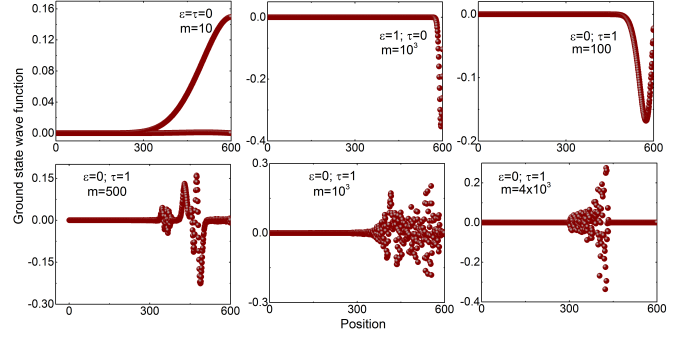


Fig. 6: Plots of ground state wave function versus radial distance of lattice for linear dispersion relation (top-left), fourth order (top center) and sixth order derivative terms for $n = 300$ and $P = 1$.

IV. DISCUSSION AND FUTURE OUTLOOK

A. What causes the quantum phase transition?

As we have shown explicitly, the sixth order derivative term leads to QPT. It is expected that the QPT should be accompanied by a fundamental change in the ground state properties of the system. To go about understanding this, in Fig. (6), we have plotted the ground state wave function of the system as a function of position (lattice point). For small m , the wave-function peaks near the boundary, however, for higher m the wave-function is more dispersed and peaks at the center. Recalling the results plotted in Fig. (3) that above the critical values of $P = 0.17$, several m have zero energy and that the wave-function peaks at the center the following physical picture emerges: For small P , there exists only one ($m = 0$) zero mode, however, as P increases the number of zero modes increase. This constitutes a fundamental change in the behavior of the system and hence leading to a phase transition.

B. Implications for high temperature superconductivity

It is natural to ask: Is there any physical system that has a long-range interaction in the 2-D plane and shows such a distinct phase transition? We shall see that it is indeed the case. More specifically, we show that our model can explain some of the experimental results of the Copper Oxide HTS. Copper Oxide HTS have 2-D layered crystal structure whose inter-atomic distance is smaller than the inter-atomic distance along the z -axis [30]. It is long-known that, in HTS, the coulombic interactions between the electrons tend to make an anti-ferromagnetic arrangement of spins in the Copper Oxide planes and the magnetic transition is controlled by the weak coupling between the planes along the z -axis [48].

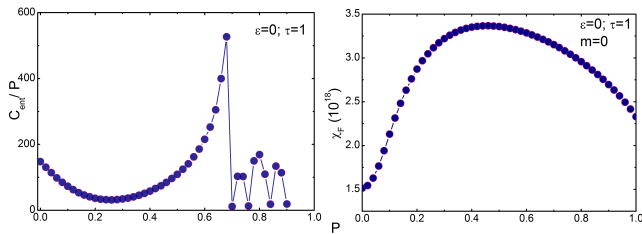


Fig. 7: Left figure is the plot of entanglement specific heat per P ($C_{ent}/P = dS_{\infty}/dP$) versus P obtained from the single copy entanglement entropy (S_{∞} is the Rényi entropy having infinity as the Rényi index). Right figure is the plot of fidelity susceptibility ($\chi_F = \lim_{\delta P \rightarrow 0} -2 \log F / \delta P^2$) as a function of P . We have taken lattice size of the z -axis to be 10 times more than the lattice size of the 2-dimensional surface, $N = 600, n = 300$ and $\delta P = 10^{-9}$.

To overcome the complexity of the interactions, we consider a scalar order parameter Φ in 3-dimensional cylindrical geometry such that the higher derivative terms contribute only in the 2-dimensional plane while the first derivative term contribute acts in all the three spatial dimensions. Repeating the analysis in 3-dimensions, it can be shown that the model in 3-dimensions has the same entropy profile as that in the 2-dimensional case (for detailed calculations, see Ref. [37]). In Fig. (7), we have plotted entanglement specific heat and fidelity susceptibility as a function of P (see the text below the Fig. (7)). Following points are interesting to note: First, the entanglement specific heat shows discontinuity at a particular value of P . This is indeed similar to the discontinuity of the specific heat measurement of the single crystals of $\text{YBa}_2\text{Cu}_3\text{O}_{7-\delta}$ [30]. Second, discontinuity of the entanglement specific heat at, say, P_0 implies that the correlation length diverges close to P_0 . For instance, in the case of transverse quantum Ising model, entanglement specific heat diverges logarithmically [6] that signals the correlation length to diverge. In our case, the entanglement specific heat diverges more like power-law. Third, it is interesting to see how our model fares with the specific heat measurements at extreme high magnetic fields as recently reported by Badoux et al [49].

We would like to conclude by reminding once again about the debate whether the LGW theory of phase transition is adequate to understand QPT. Our analysis explicitly shows that this is indeed the case as Landau theory requires nonlinear term to drive transition. In our model, QPT is driven by higher derivative term. While the model proposed here is a simple scalar order parameter, it can explain some of the crucial experimental measurements including the discontinuity [50]. Our goal is to include charge carriers in the model including sixth derivative term and explain other phenomena in the HTS. We hope to report this in the future.

Acknowledgments

We thank G. Baskaran for helpful discussions and collaboration in the initial stage of the work. Also, it is our pleasure to acknowledge Jens Eisert, Diptiman Sen, and G. Venketeswara Pai for fruitful discussion and interesting comments. We are also grateful to the organizers and participants of the conference “Information Universe” held in Groningen, The Netherlands, where important progress was made. All numerical codes were run in the fast computing clusters at IISER-TVM. SSK is supported by Senior Research Fellowship of the CSIR, Govt. of India. This work is supported by Max Planck-India Partner Group on Gravity and Cosmology.

Appendix A: Evaluation of entanglement entropy in 2-dimensional space

We consider the following $(2+1)$ - dimensional Hamiltonian;

$$\hat{H} = \frac{1}{2} \int d^2 \mathbf{r} \left[\hat{\Pi}^2(\mathbf{r}) + \left| \nabla \hat{\Phi}(\mathbf{r}) \right|^2 + \frac{\epsilon}{\kappa^2} \left| \nabla^2 \hat{\Phi}(\mathbf{r}) \right|^2 + \frac{\tau}{\kappa^4} \left| \nabla^3 \hat{\Phi}(\mathbf{r}) \right|^2 \right] \quad (\text{A1})$$

where $\hat{\Phi}$ is the order parameter and $\hat{\Pi}$ is its conjugate momenta, ϵ and τ are dimensionless constants, κ has the dimension of wave number and $\mathbf{r}(=r, \theta)$ is the circular polar coordinates. All the computations are done in by setting $\hbar = c = 1$.

The equal time canonical commutation relation between fields, which are the functions of \mathbf{r} is given by,

$$\left[\hat{\Phi}(\mathbf{r}), \hat{\Pi}(\mathbf{r}') \right] = i \delta^2(\mathbf{r} - \mathbf{r}') = \frac{i}{r} \delta(r - r') \delta(\theta - \theta') \quad (\text{A2})$$

We use the following ansatz for expanding the real scalar fields in circular polar coordinates

$$\hat{\Pi}(\mathbf{r}) = \sum_{m=-\infty}^{\infty} \frac{\hat{\Pi}_m(r)}{\sqrt{\pi r}} \cos m\theta \quad (\text{A3a})$$

$$\hat{\Phi}(\mathbf{r}) = \sum_{m=-\infty}^{\infty} \frac{\hat{\varphi}_m(r)}{\sqrt{\pi r}} \cos m\theta, \quad (\text{A3b})$$

where m is the angular momentum quantum number. The canonical commutation relation between the new rescaled fields is

$$\left[\hat{\varphi}_m(r), \hat{\Pi}_{m'}(r') \right] = i \delta(r - r') \delta_{mm'} \quad (\text{A4})$$

Integration over the polar angle θ is carried out by invoking the orthogonal properties of the cosine function and follow the central difference scheme discretization of radius on a radial lattice having N lattice points with a is the lattice parameter, the Hamiltonian in eq. (A1) becomes,

$$\begin{aligned} \hat{H} = & \frac{1}{2a} \sum_{m=-\infty}^{\infty} \sum_{j=1}^N \left[\hat{\pi}_{m,j}^2 + \left(\frac{\hat{\varphi}_{m,j+1} - \hat{\varphi}_{m,j-1}}{2} \right)^2 - \frac{\hat{\varphi}_{m,j}}{2j} (\hat{\varphi}_{m,j+1} - \hat{\varphi}_{m,j-1}) + (1 + 4m^2) \frac{\hat{\varphi}_{m,j}^2}{j^2} \right. \\ & + \frac{\epsilon}{P} \left\{ (\hat{\varphi}_{m,j+1} - 2\hat{\varphi}_{m,j} + \hat{\varphi}_{m,j-1})^2 + \frac{2\beta}{j^2} (\hat{\varphi}_{m,j+1} - 2\hat{\varphi}_{m,j} + \hat{\varphi}_{m,j-1})^2 + \frac{\beta^2}{j^4} \hat{\varphi}_{m,j}^2 \right\} \\ & + \frac{\tau}{P^2} \left\{ \left(\frac{\hat{\varphi}_{m,j+2} - 2\hat{\varphi}_{m,j+1} + 2\hat{\varphi}_{m,j-1} - \hat{\varphi}_{m,j-2}}{2} \right)^2 + \frac{\alpha}{j^2} (\hat{\varphi}_{m,j+1} - 2\hat{\varphi}_{m,j} + \hat{\varphi}_{m,j-1})^2 \right. \\ & + \frac{\beta^2}{j^4} \left(\frac{\hat{\varphi}_{m,j+1} - \hat{\varphi}_{m,j-1}}{2} \right)^2 + \frac{25/4 + m^2}{j^6} \beta^2 \hat{\varphi}_{m,j}^2 - \frac{5\beta^2}{2j^5} \left(\frac{\hat{\varphi}_{m,j+1} - \hat{\varphi}_{m,j-1}}{2} \right) \hat{\varphi}_{m,j} \\ & - \left(\frac{\hat{\varphi}_{m,j+2} - 2\hat{\varphi}_{m,j+1} + 2\hat{\varphi}_{m,j-1} - \hat{\varphi}_{m,j-2}}{2j} \right) (\hat{\varphi}_{m,j+1} - 2\hat{\varphi}_{m,j} + \hat{\varphi}_{m,j-1}) \\ & + \frac{2\beta}{j^2} \left(\frac{\hat{\varphi}_{m,j+2} - 2\hat{\varphi}_{m,j+1} + 2\hat{\varphi}_{m,j-1} - \hat{\varphi}_{m,j-2}}{2} \right) \left(\frac{\hat{\varphi}_{m,j+1} - \hat{\varphi}_{m,j-1}}{2} \right) \\ & - \frac{5\beta}{j^3} \left(\frac{\hat{\varphi}_{m,j+2} - 2\hat{\varphi}_{m,j+1} + 2\hat{\varphi}_{m,j-1} - \hat{\varphi}_{m,j-2}}{2} \right) \hat{\varphi}_{m,j} - \frac{\beta}{j^3} (\hat{\varphi}_{m,j+1} - 2\hat{\varphi}_{m,j} + \hat{\varphi}_{m,j-1}) \\ & \left. \times \left(\frac{\hat{\varphi}_{m,j+1} - \hat{\varphi}_{m,j-1}}{2} \right) + \frac{(5/2 + 2m^2) \beta}{j^4} (\hat{\varphi}_{m,j+1} - 2\hat{\varphi}_{m,j} + \hat{\varphi}_{m,j-1}) \hat{\varphi}_{m,j} \right\} \quad (\text{A5}) \end{aligned}$$

where $\pi_{m,j} = a \Pi_{m,j}$ is the new canonical momentum field, and $\hat{\varphi}_{m,N+1} = 0$ is the constraint on field.

The canonical commutation relation between the dimensionless fields is

$$[\hat{\varphi}_{m,j}, \hat{\pi}_{m',j'}] = i \delta_{mm'} \delta_{jj'} \quad (\text{A6})$$

More explicitly we can write the above interacting quantum Hamiltonian as a set of N coupled harmonic oscillators with time independent frequency as [38, 39],

$$H(P) = \frac{1}{2a} \sum_{m=-\infty}^{\infty} \sum_{i,j=1}^N [\pi_{m,i}^2 \delta_{i,j} + \phi_{m,i} K_{ij}(P, m) \phi_{m,j}] \quad (\text{A7})$$

where K_{ij} is a real symmetric interaction matrix have positive real energy eigenvalues and is given by,

$$\begin{aligned} K_{ij}(P, m) = & \left[\left(\frac{1}{4} + \frac{\alpha}{j^2} \right) + \epsilon P \left(5 - \frac{4\beta}{j^2} + \frac{\beta^2}{j^4} \right) + \tau P^2 \left(\frac{3}{4} + \frac{17\alpha}{(j+1)^2} + \frac{\gamma\beta^2}{j^6} - \frac{2\delta\beta}{j^4} - \frac{3\beta}{2(j+1)^3} \right. \right. \\ & \left. \left. + \frac{\beta^2}{4(j+1)^4} \right) \right] \delta_{j1} + \left[\left(\frac{1}{2} + \frac{\alpha}{j^2} \right) + \epsilon P \left(6 - \frac{4\beta}{j^2} + \frac{\beta^2}{j^4} \right) + \tau P^2 \left(\frac{35}{12} + \frac{19\alpha}{(j+1)^2} + \frac{\gamma\beta^2}{j^6} \right. \right. \\ & \left. \left. - \frac{2\delta\beta}{j^4} - \frac{43\beta}{(j+1)^3} + \frac{82\beta^2}{4(j+1)^4} \right) \right] \delta_{j2} + \left[\left(\frac{1}{2} + \frac{\alpha}{j^2} \right) + \epsilon P \left(6 - \frac{4\beta}{j^2} + \frac{\beta^2}{j^4} \right) + \tau P^2 \left(\frac{5}{2} \right. \right. \\ & \left. \left. + \frac{2}{j^2 - 1} + (\alpha - \beta) \left(\frac{1}{(j+1)^2} + \frac{1}{(j-1)^2} \right) + \frac{\beta^2}{4} \left(\frac{1}{(j+1)^4} + \frac{1}{(j-1)^4} \right) + \frac{4\alpha}{j^2} \right. \right. \\ & \left. \left. + \frac{\gamma\beta^2}{j^6} - \frac{2\delta\beta}{j^4} + \frac{\beta}{2} \left(\frac{1}{(j+1)^3} - \frac{1}{(j-1)^3} + \frac{\beta}{2(j+1)^4} \right) \right) \right] \delta_{ij(j \neq 1, 2, N-1, N)} \\ & + \left[\left(\frac{1}{2} + \frac{\alpha}{(N-1)^2} \right) + \epsilon P \left(6 - \frac{4\beta}{(N-1)^2} + \frac{\beta^2}{(N-1)^4} \right) + \tau P^2 \left(\frac{9}{4} + \frac{2}{(N-2)N} \right. \right. \\ & \left. \left. + (\alpha - \beta) \left(\frac{1}{(N-2)^2} + \frac{1}{N^2} \right) + \frac{\beta^2}{4} \left(\frac{1}{(N-2)^4} + \frac{1}{N^4} \right) + \frac{4\alpha}{(N-1)^2} + \frac{\gamma\beta^2}{(N-1)^6} \right. \right. \\ & \left. \left. - \frac{2\delta\beta}{(N-1)^4} + \frac{\beta}{2} \left(\frac{1}{N^3} - \frac{1}{(N-1)^3} + \frac{\beta}{2N^4} \right) \right) \right] \delta_{iN-2} + \left[\left(\frac{1}{4} + \frac{\alpha}{N^2} \right) + \epsilon P \left(5 - \frac{4\beta}{N^2} \right. \right. \\ & \left. \left. + \frac{\beta^2}{N^4} \right) + \tau P^2 \left(\frac{5N+1}{4(N-2)} + \frac{\alpha - \beta}{(N-1)^2} + \frac{\beta^2}{4(N-1)^4} - \frac{\beta}{2(N-1)^3} + \frac{\gamma\beta^2}{N^6} - \frac{2\beta\delta}{N^4} \right) \right] \delta_{i,N} \\ & + \left[-\frac{1}{8} + \epsilon P \left(\frac{5\beta}{4} - 4 \right) + \frac{\tau P^2}{2} \left(\frac{-11}{6} - 5\alpha + \frac{191\beta}{36} + \frac{17\beta\delta}{16} - \frac{155\beta^2}{64} \right) \right] \delta_{i,j-1(j=2)} \\ & + \left[\frac{-1}{8} + \epsilon P \left(\frac{5\beta}{4} - 4 \right) + \frac{\tau P^2}{2} \left(\frac{-11}{6} - 5\alpha + \frac{191\beta}{36} + \frac{17\beta\delta}{16} - \frac{155\beta^2}{64} \right) \right] \delta_{i,j+1(j=1)} \\ & + \left[-\frac{1}{4i(i+1)} + \epsilon P \left(-4 + \beta \left(\frac{1}{i^2} + \frac{1}{(i+1)^2} \right) \right) + \frac{\tau P^2}{2} \left(-2 - \frac{3}{(i-1)(i+2)} \right. \right. \\ & \left. \left. - \frac{1}{i(i+1)} + \frac{\beta}{2(i-1)^2} - \frac{4\alpha}{i^2} + \frac{\delta\beta}{i^4} + \frac{6\beta}{i^3} - \frac{5\beta^2}{2i^5} - \frac{4\alpha}{(i+1)^2} + \frac{\delta\beta}{(i+1)^4} + \frac{6\beta}{(i+1)^3} \right. \right. \\ & \left. \left. - \frac{5\beta^2}{2(i+1)^5} - \frac{4\alpha}{(i+1)^2} + \frac{\beta}{2(i+1)^2} + \delta_{iN-1} \left(1 - \frac{1}{2(N+1)} - \frac{\beta}{2(N+1)^2} \right) \right) \right] \delta_{ij+1, (i \neq 1)} \\ & + \left[-\frac{1}{4j(j+1)} + \epsilon P \left(-4 + \beta \left(\frac{1}{j^2} + \frac{1}{(j+1)^2} \right) \right) + \frac{\tau P^2}{2} \left(-2 - \frac{3}{(j-1)(j+2)} \right. \right. \\ & \left. \left. - \frac{1}{j(j+1)} + \frac{\beta}{2(j-1)^2} - \frac{4\alpha}{j^2} + \frac{\delta\beta}{j^4} + \frac{6\beta}{j^3} - \frac{5\beta^2}{2j^5} - \frac{4\alpha}{(j+1)^2} + \frac{\delta\beta}{(j+1)^4} + \frac{6\beta}{(j+1)^3} \right. \right. \\ & \left. \left. - \frac{5\beta^2}{2(j+1)^5} - \frac{4\alpha}{(j+1)^2} + \frac{\beta}{2(j+1)^2} + \delta_{jN-1} \left(1 - \frac{1}{2(N+1)} - \frac{\beta}{2(N+1)^2} \right) \right) \right] \delta_{ij-1, (j \neq 2)} \\ & + \left[-\frac{1}{4} + \epsilon P + \frac{\tau P^2}{2} \left(-2 + \frac{2\alpha}{(i+1)^2} - \frac{\beta^2}{2(i+1)^4} + \frac{2}{i(i+2)} + \frac{5\beta}{2} \left(\frac{1}{(i+2)^3} - \frac{1}{i^3} \right. \right. \right. \\ & \left. \left. \left. + \frac{4\beta}{5(i+1)^2} \right) \right) \right] \delta_{ij+2} + \left[-\frac{1}{4} + \epsilon P + \frac{\tau P^2}{2} \left(-2 + \frac{2\alpha}{(j+1)^2} - \frac{\beta^2}{2(j+1)^4} + \frac{2}{j(j+2)} \right. \right. \\ & \left. \left. + \frac{5\beta}{2} \left(\frac{1}{(j+2)^3} - \frac{1}{j^3} + \frac{4\beta}{5(j+1)^2} \right) \right) \right] \delta_{ij-2} - \frac{\tau P^2}{4} \delta_{i,j+4} - \frac{\tau P^2}{4} \delta_{i,j-4} \end{aligned}$$

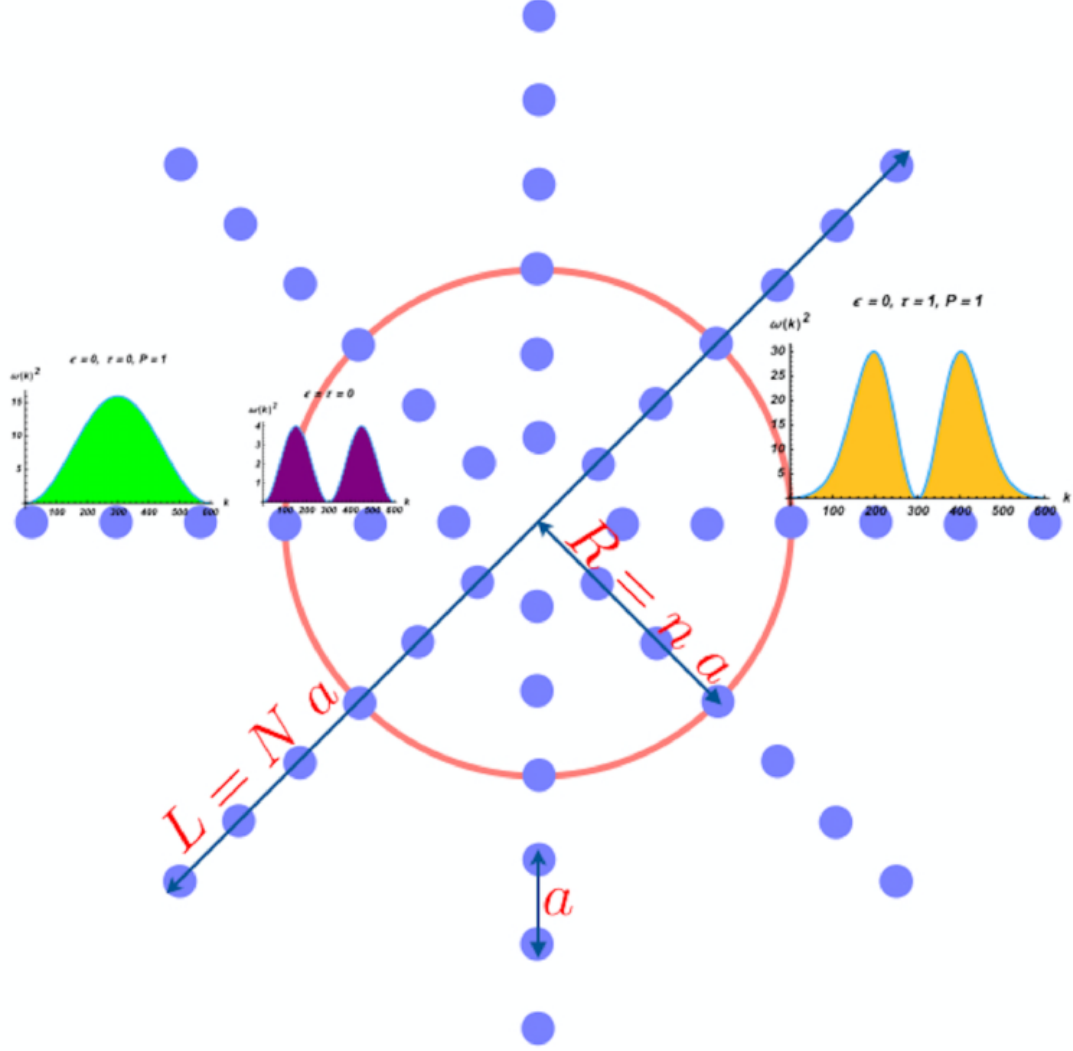


Fig. 8: Pictorial representation of radial lattice with all the interactions. The dark circles are the lattice points and different curves represent possible type of interaction among the lattice points. The reduced density matrix ρ of the subsystem correspond to the lattice points inside the Brown circle of radius R .

$$\begin{aligned}
 & + \frac{\tau P^2}{2} \left[2 - \frac{1}{(i+1)(i+2)} - \frac{\beta}{2} \left(\frac{1}{(i+1)^2} + \frac{1}{(i+2)^2} \right) \right] \delta_{ij+3} + \frac{\tau P^2}{2} \left[2 - \frac{\beta}{2} \left(\frac{1}{(j+1)^2} \right. \right. \\
 & \left. \left. + \frac{1}{(j+2)^2} \right) - \frac{1}{(j+1)(j+2)} \right] \delta_{ij-3}
 \end{aligned}$$

where

$$\alpha(m) = \frac{1+4m^2}{4}; \beta(m) = \frac{1-4m^2}{4}; \gamma(m) = \frac{25}{4} + m^2; \delta(m) = \frac{5}{2} + 2m^2 \quad (\text{A8})$$

$$P = \frac{1}{(\kappa a)^2}, \quad \text{is the cutoff scale in the system.} \quad (\text{A9})$$

The ground state wave function of the above Hamiltonian is given by,

$$\psi_{\text{GS}}(x) = \frac{1}{\pi^{N/4}} (\det \Lambda)^{1/4} \exp(-x^T \Lambda x / 2) \quad (\text{A10})$$

where $\Lambda = \sqrt{K} = \begin{pmatrix} A & B \\ B^T & C \end{pmatrix}$ and A, B, C are the sub matrices of Λ matrix with dimensions $n \times n, n \times (N-n)$ and $(N-n) \times (N-n)$ respectively and $x = (x_1, x_2, \dots, x_n, t_1, t_2, \dots, t_{N-n})^T$. The density matrix for the ground state is

$$\rho_{\text{GS}}(x, x') = \psi_{\text{GS}}(x) \psi_{\text{GS}}^*(x') \quad (\text{A11})$$

The ground state reduced density matrix, ρ is obtained by tracing over the first n of N oscillators of the pure density matrix ρ_{GS}

$$\rho(t, t') = \int \prod_{i=1}^n dx_i \psi_{\text{GS}}(x_1, x_2, \dots, x_n, t_1, t_2, \dots, t_{N-n}) \psi_{\text{GS}}^*(x_1, x_2, \dots, x_n, t_1, t_2, \dots, t_{N-n}) \quad (\text{A12})$$

where $t = (t_1, t_2, \dots, t_{N-n})^T$. The integral in Eq. (A12) can be evaluated explicitly and can be written as,

$$\rho_{\text{red}}(t, t') \sim \exp \left[-(t^T \Gamma t + t'^T \Gamma t')/2 + t^T \Omega t' \right] \quad (\text{A13})$$

where Ω and Γ are defined by

$$\Omega = \frac{1}{2} B^T A^{-1} B \quad (\text{A14a})$$

$$\Gamma = C - \beta \quad (\text{A14b})$$

Let Γ_D and V be the diagonal and orthogonal matrices of Γ and do the transformation $t = V^T \Gamma_D^{-1/2} y$ then $\Omega \rightarrow \Omega' = \Gamma_D^{-1/2} V \Omega V^T \Gamma_D^{-1/2}$ and the reduced density matrix becomes,

$$\rho_{\text{red}}(y, y') \sim \exp \left[-(y \cdot y + y' \cdot y')/2 + y^T \Omega' y' \right] \quad (\text{A15})$$

Rewriting $y = Wz$, where W is a orthogonal matrix such that Ω' is diagonal in W basis, Eq. (A15) becomes:

$$\rho_{\text{red}}(z, z') \sim \prod_{i=1}^{N-n} \exp \left[-(z_i^2 + z_i'^2)/2 + \Omega_i z_i z_i' \right] \quad (\text{A16})$$

where Ω_i is an eigenvalue of Ω' . The von Neumann entropy of the ρ_{red} is given by,

$$S_m = \sum_{i=1}^{N-n} S_{m,i}(\xi_i) \quad (\text{A17})$$

where

$$S_m(\xi) = \sum_{i=1}^{N-n} \left(\log(1 - \xi_i) - \frac{\xi_i}{1 - \xi_i} \log \xi_i \right) \quad (\text{A18a})$$

$$\xi_i = \frac{\Omega'_i}{\left[1 + (1 - \Omega'_i)^{(1/2)} \right]} \quad (\text{A18b})$$

The entanglement entropy (EE) is computed by summing over all m modes as

$$S = S_{m=0} + 2 \sum_{m=1}^{\infty} S_m \quad (\text{A19})$$

where $S_{m=0}$ is the value of EE for $m = 0$ and all other S_m values are multiplied by the degeneracy factor 2. Figure (9) contains the plot of EE versus n for the linear dispersion relation ($\omega = k$) and $\omega^2 = k^2 + k^4/\kappa^2$. In all the computations, we use an accuracy of 10^{-8} and all the matrix entries in the K_{ij} are rescaled by a factor of 10^{-10} .

It is interesting to note that EE is proportional to even in the presence of fourth order term, however, its profile completely changes due to the sixth order derivative

Appendix B: Entanglement entropy for different lattice sizes in 2- dimensional space

Figures (10) and (11) show the behaviour of entanglement entropy for different N 's and different scenarios. The area law is verified for the $\epsilon = 1, \tau = 0$ case and violation of the area law for the case $\epsilon = 1, \tau = 1$ is showed. Checking the results for different N 's show that the violation of area law of the entanglement entropy is due to the presence of the sixth order derivative.

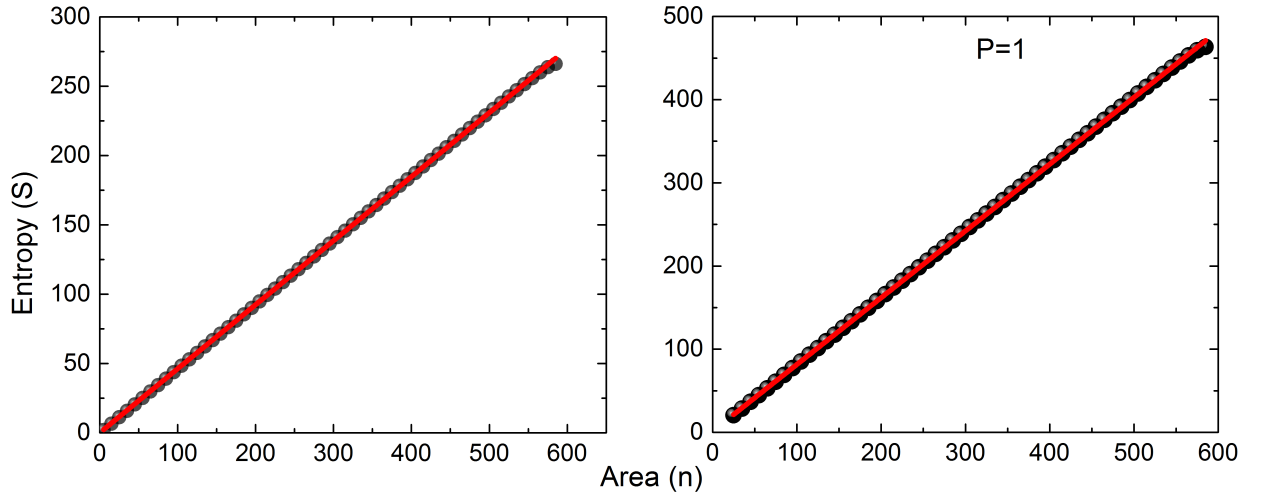


Fig. 9: Left figure is the plot of entanglement entropy (S) vs n for linear dispersion relation. Right figure is the plot of entanglement entropy (S) vs n for scenario I i. e. $\epsilon = 1, \tau = 0, P = 1, N = 600$. The black dots represent numerical data points generated by MATLAB R2012a and the red line is the best linear fit represented by the equation $S = a n + 0.038 \log n$, where a is slope of the line.

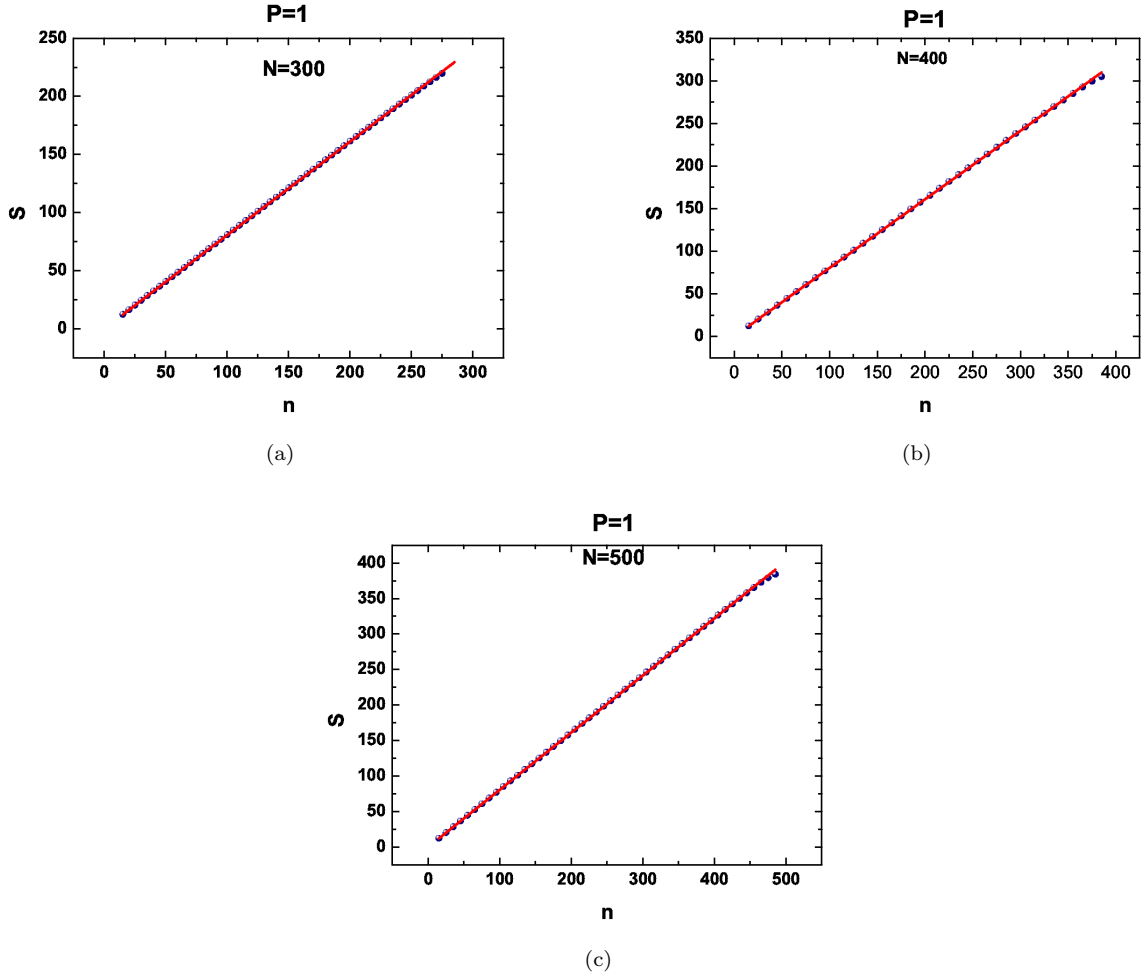


Fig. 10: Plot of entropy as a function of n for various P values for $\epsilon = 1, \tau = 0$ with $N=300, 400, 500$ sites respectively. The blue dots represents numerical data and the red lines are the best linear fit represented by $S = a n + 0.038 \log n$, where a is slope of the line.

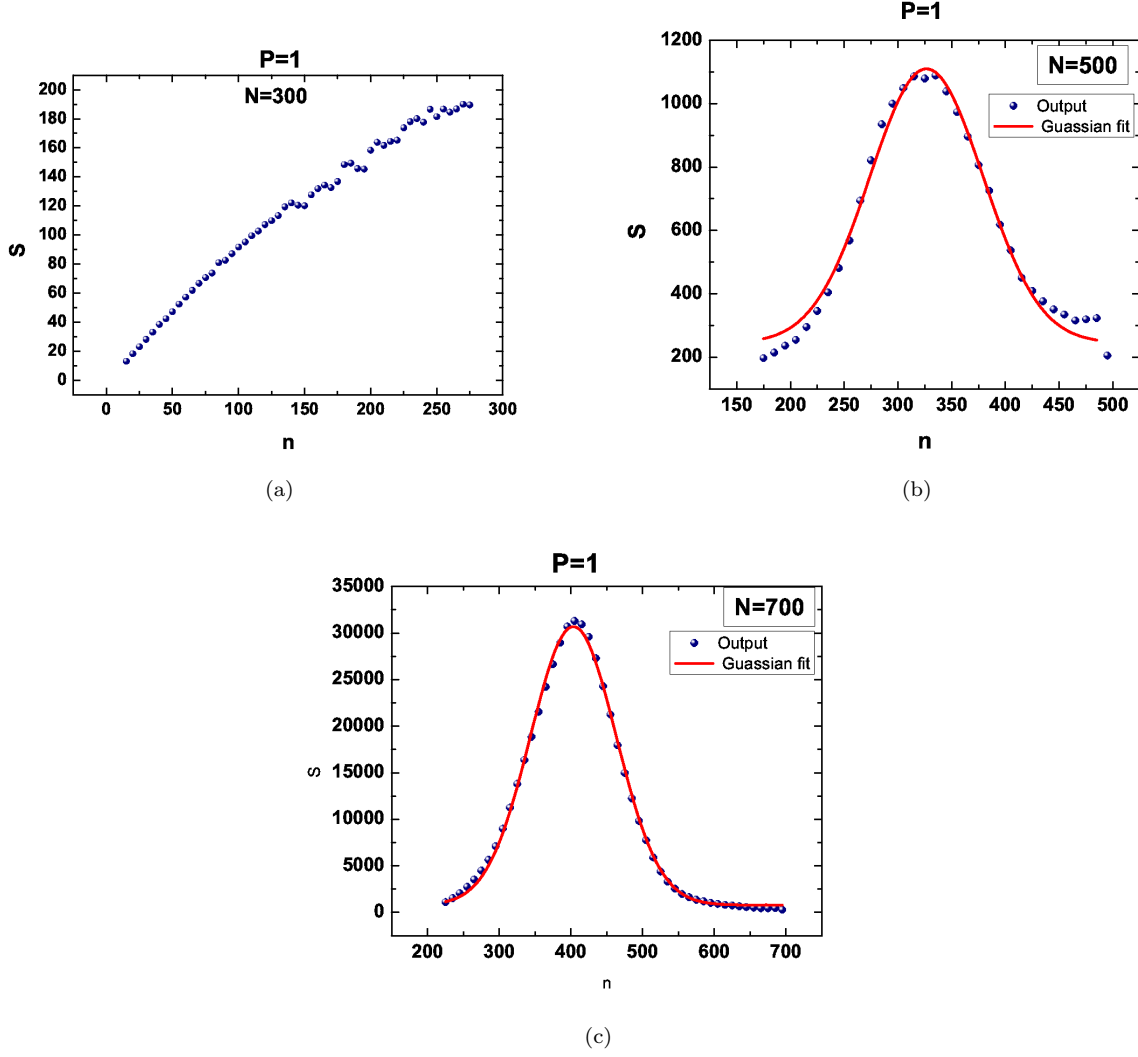


Fig. 11: Plot of entropy as a function of n for various P values for $\epsilon = 1, \tau = 1$ with $N = 300, 500, 700$ sites, respectively. The blue dots represent the output and the red colour is the best fit.

Appendix C: Entanglement entropy of scalar field in cylindrical geometry

The Hamiltonian in the 3-dimensional cylindrical geometry is given by:

$$\hat{H}_1 = \frac{1}{2} \int d^2 \mathbf{r} dz \left[\hat{\Pi}^2(\mathbf{r}, z) + \left| \nabla \hat{\Phi}(\mathbf{r}, z) \right|^2 + \frac{\epsilon}{\kappa^2} \left| \nabla_{\mathbf{r}}^2 \hat{\Phi}(\mathbf{r}, z) \right|^2 + \frac{\tau}{\kappa^4} \left| \nabla_{\mathbf{r}}^3 \hat{\Phi}(\mathbf{r}, z) \right|^2 \right] \quad (\text{C1})$$

where $\hat{\Phi}$ and $\hat{\Pi}$ are the one component real massless scalar field and its conjugate momenta respectively, ϵ and τ are dimensionless constants, κ has the dimension of wave number and $\mathbf{r}(= r, \theta)$ is the circular polar coordinates and z is the height of the cylinder. Here $\nabla_{\mathbf{r}}^2$ and $\nabla_{\mathbf{r}}^3$ represent higher order derivative operators for the 2-D plane. That is we study the effect of the higher derivative terms in the 2-D plane — interaction strength is comparatively less in the z direction.

The equal time canonical commutation relation between fields, which are the functions of \mathbf{r} and z is given by,

$$\left[\hat{\Phi}(\mathbf{r}, z), \hat{\Pi}(\mathbf{r}', z) \right] = i \delta^2(\mathbf{r} - \mathbf{r}') \delta(z - z') = \frac{i}{r} \delta(r - r') \delta(\theta - \theta') \delta(z - z') \quad (\text{C2})$$

We use the following ansatz for expanding the real scalar fields in circular cylindrical coordinates

$$\hat{\Pi}(\mathbf{r}, z) = \frac{1}{2\pi^2} \int_0^\infty dk \sum_{m=-\infty}^\infty \frac{\hat{\Pi}_m(r, k)}{\sqrt{r}} \cos m\theta \cos kz \quad (\text{C3a})$$

$$\hat{\Phi}(\mathbf{r}, z) = \frac{1}{2\pi^2} \int_0^\infty dk \sum_{m=-\infty}^\infty \frac{\hat{\Phi}_m(r, k)}{\sqrt{r}} \cos m\theta \cos kz, \quad (\text{C3b})$$

where m is the angular momentum quantum number and k is a real positive parameter which has the dimension of momentum. The canonical commutation relation between the new rescaled fields is

$$[\hat{\Phi}_m(r, k), \hat{\Pi}_{m'}(r', k')] = i \delta(r - r') \delta(k - k') \delta_{mm'} \quad (\text{C4})$$

Unlike in the case of circular polar coordinates, here we have to do two different discretization —one for the radial direction and other along in the height of the cylinder. For numerical simplicity, we choose the height of the cylinder is some arbitrary number ν times its radius. Let a and b are the lattice parameter in the radial and z - direction respectively and here we takes $b = \nu a$. That is,

$$r = ja; \quad 1/k = s \nu a \quad (\text{C5})$$

After some little algebra, we can write the total Hamiltonian in the following form;

$$\begin{aligned} \hat{H}_1 = & \frac{1}{2a} \sum_{s=1}^{N_1} \sum_{m=-\infty}^\infty \sum_{j=1}^N \left[\hat{\Xi}_{m,j,s}^2 + \left(\frac{\hat{\chi}_{m,j+1,s} - \hat{\chi}_{m,j-1,s}}{2} \right)^2 - \frac{\hat{\chi}_{m,j,s}}{2j} (\hat{\chi}_{m,j+1,s} - \hat{\chi}_{m,j-1,s}) \right. \\ & + (1 + 4m^2) \frac{\hat{\chi}_{m,j,s}^2}{j^2} + \frac{1}{s^2 \nu^2} \hat{\chi}_{m,j,s}^2 \\ & + \frac{\epsilon}{P} \left\{ (\hat{\chi}_{m,j+1,s} - 2\hat{\chi}_{m,j,s} + \hat{\chi}_{m,j-1,s})^2 + \frac{2\beta}{j^2} (\hat{\chi}_{m,j+1,s} - 2\hat{\chi}_{m,j,s} + \hat{\chi}_{m,j-1,s})^2 + \frac{\beta^2}{j^4} \hat{\chi}_{m,j,s}^2 \right\} \\ & + \frac{\tau}{P^2} \left\{ \left(\frac{\hat{\chi}_{m,j+2,s} - 2\hat{\chi}_{m,j+1,s} + 2\hat{\chi}_{m,j-1,s} - \hat{\chi}_{m,j-2,s}}{2} \right)^2 + \frac{\alpha}{j^2} (\hat{\chi}_{m,j+1,s} - 2\hat{\chi}_{m,j,s} + \hat{\chi}_{m,j-1,s})^2 \right. \\ & + \frac{\beta^2}{j^4} \left(\frac{\hat{\chi}_{m,j+1,s} - \hat{\chi}_{m,j-1,s}}{2} \right)^2 + \frac{25/4 + m^2}{j^6} \beta^2 \hat{\chi}_{m,j,s}^2 - \frac{5\beta^2}{2j^5} \left(\frac{\hat{\chi}_{m,j+1,s} - \hat{\chi}_{m,j-1,s}}{2} \right) \hat{\chi}_{m,j,s} \\ & - \left(\frac{\hat{\chi}_{m,j+2,s} - 2\hat{\chi}_{m,j+1,s} + 2\hat{\chi}_{m,j-1,s} - \hat{\chi}_{m,j-2,s}}{2j} \right) (\hat{\chi}_{m,j+1,s} - 2\hat{\chi}_{m,j,s} + \hat{\chi}_{m,j-1,s}) \\ & + \frac{2\beta}{j^2} \left(\frac{\hat{\chi}_{m,j+2,s} - 2\hat{\chi}_{m,j+1,s} + 2\hat{\chi}_{m,j-1,s} - \hat{\chi}_{m,j-2,s}}{2} \right) \left(\frac{\hat{\chi}_{m,j+1,s} - \hat{\chi}_{m,j-1,s}}{2} \right) \\ & - \frac{5\beta}{j^3} \left(\frac{\hat{\chi}_{m,j+2,s} - 2\hat{\chi}_{m,j+1,s} + 2\hat{\chi}_{m,j-1,s} - \hat{\chi}_{m,j-2,s}}{2} \right) \hat{\chi}_{m,j,s} - \frac{\beta}{j^3} (\hat{\chi}_{m,j+1,s} - 2\hat{\chi}_{m,j,s} + \hat{\chi}_{m,j-1,s}) \\ & \left. \times \left(\frac{\hat{\chi}_{m,j+1,s} - \hat{\chi}_{m,j-1,s}}{2} \right) + \frac{(5/2 + 2m^2)\beta}{j^4} (\hat{\chi}_{m,j+1,s} - 2\hat{\chi}_{m,j,s} + \hat{\chi}_{m,j-1,s}) \hat{\chi}_{m,j,s} \right\} \end{aligned} \quad (\text{C6})$$

where $\Xi_{m,j} = \sqrt{a} \Pi_{m,j}$ is the new canonical momentum field, $\chi_{m,j} = \varphi_{m,j,p}/\sqrt{a}$ is the new dimensionless scalar field, N_1 and N are the lattice points along the radial, z directions respectively and $\chi_{m,N_1+1} = 0, \chi_{m,N+1} = 0$, are the constraints on field. Thus the above Hamiltonian can be bring into a form of system of coupled HO's;

$$H_1(P) = \frac{1}{2a} \sum_{s=1}^\infty \sum_{m=-\infty}^{N_1} \sum_{i,j=1}^N [\Xi_{m,s,i}^2 \delta_{i,j} + \chi_{m,s,i} T_{ij}(P, m, s) \chi_{m,s,j}] \quad (\text{C7})$$

where $T_{ij}(P, m, s) = K_{ij}(P, m) + (s \nu)^{-2} \delta_{i,j}$ is a real symmetric interaction matrix have positive real energy eigenvalues. Using the same procedure, we obtain ground state entanglement entropy. Fig. 12 contains the plot of entanglement entropy versus area for scenario I and II .

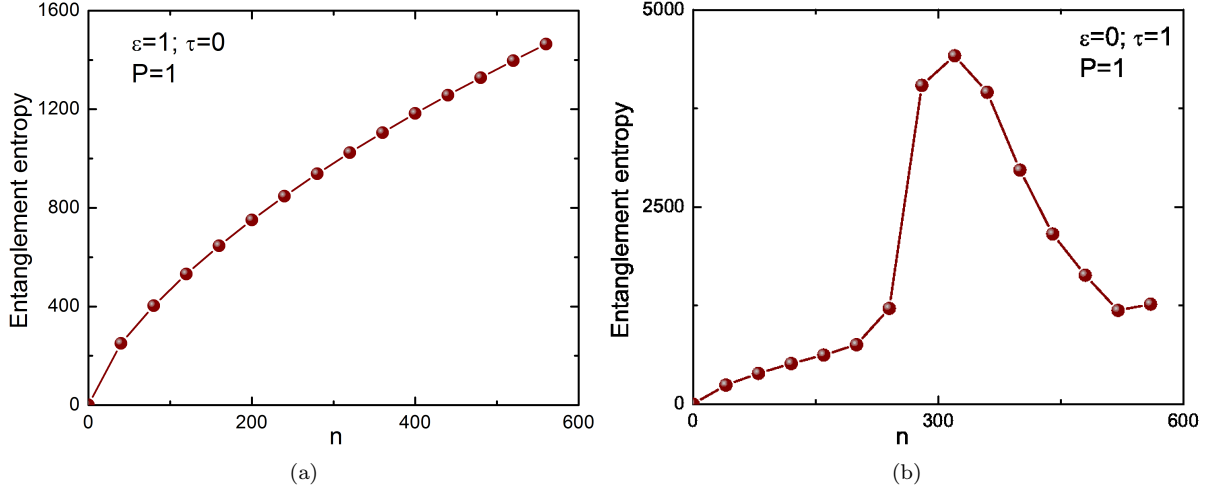


Fig. 12: Left figure is the plot of entanglement entropy versus area for scenario I. Right figure is the plot of entanglement entropy versus area for scenario II. We have used the lattice size in the z-axis is 10 times the lattice size in the 2-D plane. The number of lattice points used in the calculation are $N = 600, N_1 = 2, \delta P = 10^{-9}$ and the accuracy is 10^{-2} .

Appendix D: Specific heat from entanglement entropy

The definition of the Rényi entropy is

$$S_\varsigma = \frac{1}{1-\varsigma} \log \text{Tr } \rho^\varsigma \quad (\text{D1})$$

where ς is the Rényi parameter and $\varsigma \rightarrow 1$ gives back the von-Neumann entanglement entropy. $S_{\varsigma \rightarrow \infty}$ is referred in the literature as single copy entanglement entropy [51] and quantifies quantum correlations in the quantum ground state of the many body systems. The single copy entanglement entropy is given by,

$$S_{m,s,\varsigma \rightarrow \infty} = - \sum_{i=1}^{N-n} \log(1 - \xi_i) \quad (\text{D2})$$

where ξ_i has the same structure as that in the circular case and is obtained from $T_{ij}(P, m, s)$.

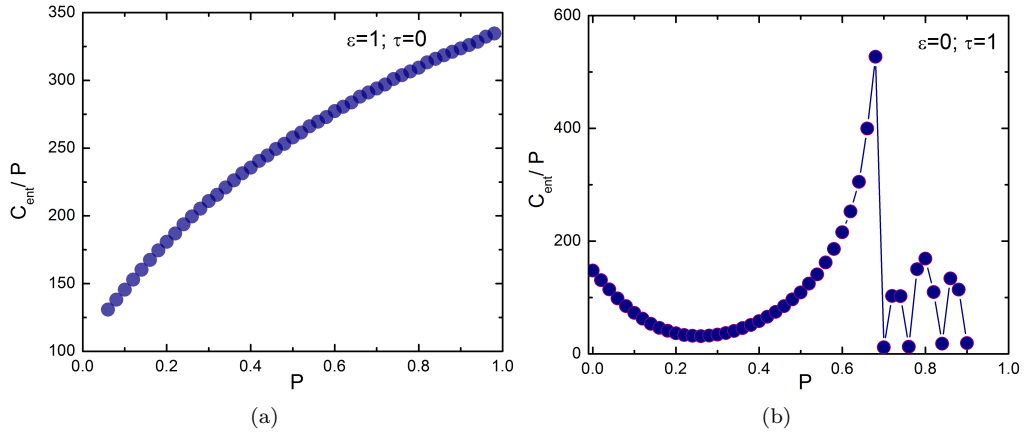


Fig. 13: Left plot is the entanglement specific heat (C_{ent}) versus P obtained from the single copy entanglement entropy. The right plot is the for the fidelity susceptibility as a function of P . We have taken lattice size of the z-axis to be 5 times more than the lattice size of the 2-dimensional surface, $N = 600$ and $n = 300$.

It has been interpreted that there has been a close resemblance between the single copy entanglement entropy and the thermodynamic entropy [52, 53]. One can define entanglement specific heat as,

$$C_{ent} = P \frac{dS_{\zeta \rightarrow \infty}}{dP} \quad (D3)$$

Appendix E: Fidelity susceptibility

Fidelity susceptibility is defined as

$$\chi_F = \lim_{\delta P \rightarrow 0} \left[-2 \frac{\log F}{\delta P^2} \right] \quad (E1)$$

where $F = \langle \psi_{1GS}(P + \delta P) | \psi_{1GS}(P) \rangle$ is the fidelity of system and ψ_{1GS} is the ground state wave function of the Hamiltonian H_1 .

-
- [1] L. D. Landau and E. M. Lifshitz, *Statistical Physics*, vol. V of *Course of Theoretical Physics* (Elsevier, 1980), 3rd ed.
 - [2] H. E. Stanley, *Introduction to Phase Transitions and Critical Phenomena* (Oxford University Press, 1987).
 - [3] J. A. Hertz, Phys. Rev. B **14**, 1165 (1976).
 - [4] T. Senthil, A. Vishwanath, L. Balents, S. Sachdev, and M. P. A. Fisher, Science **303**, 1490 (2004), ISSN 0036-8075.
 - [5] T. Vojta, Annalen der Physik **9**, 403 (2000).
 - [6] A. Osterloh, L. Amico, G. Falci, and R. Fazio, Nature **416**, 608 (2002).
 - [7] J. A. Dunningham, Nat Phys. **5**, 381 (2002).
 - [8] M. Vojta, Reports on Progress in Physics **66**, 2069 (2003).
 - [9] G. Vidal, J. I. Latorre, E. Rico, and A. Kitaev, Phys. Rev. Lett. **90**, 227902 (2003).
 - [10] L. Amico, R. Fazio, A. Osterloh, and V. Vedral, Rev. Mod. Phys. **80**, 517 (2008).
 - [11] S. Sachdev, *Quantum Phase Transitions* (Cambridge University Press, 2011), 2nd ed.
 - [12] L. Carr, *Understanding quantum phase transitions* (CRC Press, Boca Raton, 2011), 1st ed.
 - [13] G. G. Batrouni and R. T. Scalettar, “*Quantum phase transitions*” in *Ultracold Gases and Quantum Information* (Oxford University Press, 2011).
 - [14] P. Calabrese and J. Cardy, International Journal of Quantum Information **04**, 429 (2006).
 - [15] T. J. Osborne and M. A. Nielsen, Phys. Rev. A **66**, 032110 (2002).
 - [16] D. Larsson and H. Johannesson, Phys. Rev. Lett. **95**, 196406 (2005).
 - [17] T. Giamarchi, *Quantum Physics in One Dimension* (Oxford University Press, 2003).
 - [18] R. G. Unanyan and M. Fleischhauer, Phys. Rev. Lett. **95**, 260604 (2005).
 - [19] T. Barthel, M.-C. Chung, and U. Schollwöck, Phys. Rev. A **74**, 022329 (2006).
 - [20] M. Cramer, J. Eisert, and M. B. Plenio, Phys. Rev. Lett. **98**, 220603 (2007).
 - [21] P. Coleman and A. J. Schofield, Nature **433**, 226 (2005).
 - [22] S. Sachdev, Nat Phys **4**, 173 (2008).
 - [23] S.-J. GU, International Journal of Modern Physics B **24**, 4371 (2010).
 - [24] I. Peschel, Brazilian Journal of Physics **42**, 267 (2012).
 - [25] H. Li and F. D. M. Haldane, Phys. Rev. Lett. **101**, 010504 (2008).
 - [26] A. Chandran, V. Khemani, and S. L. Sondhi, Phys. Rev. Lett. **113**, 060501 (2014).
 - [27] G. De Chiara, L. Lepori, M. Lewenstein, and A. Sanpera, Phys. Rev. Lett. **109**, 237208 (2012).
 - [28] S. M. Giampaolo, S. Montangero, F. Dell’Anno, S. De Siena, and F. Illuminati, Phys. Rev. B **88**, 125142 (2013).
 - [29] R. Lundgren, J. Blair, M. Greiter, A. Läuchli, G. A. Fiete, and R. Thomale, Phys. Rev. Lett. **113**, 256404 (2014).
 - [30] N. Overend, M. A. Howson, and I. D. Lawrie, Phys. Rev. Lett. **72**, 3238 (1994).
 - [31] R. Hott, R. Kleiner, T. Wolf, and G. Zwicknagl, *Review on Superconducting Materials*, Applied Superconductivity: Handbook on Devices and Applications (Wiley-VCH Verlag GmbH & Company KGaA, 2015), ISBN 9783527670635.
 - [32] R. M. Hornreich, M. Luban, and S. Shtrikman, Phys. Rev. Lett. **35**, 1678 (1975).
 - [33] S. Ghosh and S. Shankaranarayanan, Phys. Rev. D **86**, 125011 (2012).
 - [34] S. Coleman, Comm. Math. Phys. **31**, 259 (1973).
 - [35] A. Klein, L. Landau, and D. Shucker, Journal of Statistical Physics **26**, 505 (1981).
 - [36] A. Gelfert and W. Nolting, Journal of Physics: Condensed Matter **13**, R505 (2001).
 - [37] See Supplemental Material at [URL will be inserted by publisher] for more details about the derivation of interaction matrix K_{ij} in 2D plane as well as 3D cylindrical space. (???)
 - [38] L. Bombelli, R. K. Koul, J. Lee, and R. D. Sorkin, Phys. Rev. D **34**, 373 (1986).
 - [39] M. Srednicki, Phys. Rev. Lett. **71**, 666 (1993).
 - [40] H.-H. Lai, K. Yang, and N. E. Bonesteel, Phys. Rev. Lett. **111**, 210402 (2013).

- [41] P. W. Anderson, Phys. Rev. Lett. **18**, 1049 (1967).
 - [42] M. A. Nielsen and I. L. Chuang, *Quantum Computation and Quantum Information* (Cambridge University Press, 2011), 10th ed.
 - [43] P. Zanardi and N. Paunković, Phys. Rev. E **74**, 031123 (2006).
 - [44] H.-Q. Zhou and J. P. Barjaktarevi, Journal of Physics A: Mathematical and Theoretical **41**, 412001 (2008).
 - [45] V. R. Vieira, Journal of Physics: Conference Series **213**, 012005 (2010).
 - [46] R. Thomale, A. Sterdyniak, N. Regnault, and B. A. Bernevig, Phys. Rev. Lett. **104**, 180502 (2010).
 - [47] R. Thomale, D. P. Arovas, and B. A. Bernevig, Phys. Rev. Lett. **105**, 116805 (2010).
 - [48] D. A. Bonn, Nat Phys **2**, 159 (2006).
 - [49] Badoux S., Tabis W., Lalibert F., Grissonnanche G., Vignolle B., Vignolles D., Bard J., Bonn D. A., Hardy W. N., Liang R., et al., Nature **531**, 210 (2016).
 - [50] M. Wieśniak, V. Vedral, and i. c. v. Brukner, Phys. Rev. B **78**, 064108 (2008).
 - [51] J. Eisert and M. Cramer, Phys. Rev. A **72**, 042112 (2005).
 - [52] K. K. R. Seroje, R. S. dela Rosa, and F. N. C. Paraan, European Journal of Physics **36**, 055051 (2015).
 - [53] J.-M. Stphan, G. Misguich, and V. Pasquier, Journal of Statistical Mechanics: Theory and Experiment **2012**, P02003 (2012).
-